Acoustic Waveguide Theory Revisited*

EARL R. GEDDES, *AES Fellow*

Livonia, MI 48154, USA

The concept of acoustic waveguides was introduced by Geddes in 1989. That paper showed how Webster's horn equation lacked a sufficient description of the wave propagation in the horn to be accurate in directivity simulations. The concept of a waveguide as a direct solution to the wave equation was shown to be capable of exact solution, free of the plane-wave assumption of Webster's equation. The original paper did not perform a complete calculation of the exact solution and in fact contained errors which have been of concern to some readers. The purpose of the present paper is to revisit the waveguide discussion and to proceed with an exact calculation of the wave propagation in an oblate spheroidal waveguide. These calculations will clear up the questions raised regarding the original paper as well as showing some new results.

0 INTRODUCTION

The acoustic waveguide paper [1] raised questions over the validity of Webster's equation for the modern genre of directivity-controlling devices. The emphasis on the horn as a directivity control device is important. It is a premise of this paper, as well as the original paper, that the primary function of a horn or waveguide is to control directivity. The loading function must not be ignored, of course, but as shown in Bauman et al. [2], the low-frequency responses of most devices limited to fitting into a common package (equal throat area, mouth area, and length) are very similar. In fact the common belief that a greater radiation resistance will result in greater output (mostly at cutoff) is not necessarily correct. This effect results from the larger mass reactance associated with the larger radiation resistance, which complicates the situation. The high-frequency response of a horn is most aptly described by its directivity response. However, the axial response and distortion characteristics are strongly affected by the means used to obtain this directivity [2]. Therefore the principal difference between acoustic loading devices is in the directivity response and the method used to obtain it, and not in the low-frequency loading effect. These conclusions are important since the primary interest of Webster's equation is to predict the loading. Little, if any, consideration is given to the wavefront shape other than to assume that it is planar and of constant amplitude and phase across its extent.

The original paper also contained a derivation of the acoustic impedance of an oblate spheroidal (OS) waveguide and a discussion of the wavefronts in such a device. Putland [3] has commented on several errors that occurred in this derivation, and Henwood [4] followed up with a restatement of these errors. The main concern presented by these critics regards the author's assertion that the OS waveguide was a one-parameter (1P) device. Putland has proven [5] that only three coordinate systems will have true 1P properties and that OS coordinates are not among them. This result was alluded to in the original paper, but was not developed with the elegance and completeness of Putland. The author completely agrees with Putland's arguments and now admits that, under Putland's strict definition of 1P waves, his original assertion that the OS waveguide was a true 1P device was incorrect.

The concept of 1P waves was adopted from the text of Morse [6] which, to the author's knowledge, first presented the idea of 1P waves in a horn. This discussion and the author's earlier work on horn simulations [7] led to the investigation of the waveguide approach. The 1P concept was used since it was a convenient way of describing the wavefront criteria in the derivation of the general waveguide theory. By invoking the 1P assumptions, many simplifications could be made in the derivations of the equations. These simplifications

*Manuscript received 1992 December 4; revised 1993 April 2.

were used in the original work, and as such the error of incorrectly assuming 1P waves has shed some doubt on the validity of the equations (in particular Eqs. 20 and 21 in [1]). It is important to note that the 1P concept is not required in the waveguide theory, and abandoning it does not limit the theory in any way. Eliminating the 1P assumption does, however, complicate things, as this paper will show.

The purpose of the present paper thus becomes:

1) To derive the exact equations for the OS waveguide, taking into account the concerns raised by the critics

2) To develop solutions to these equations for a number of OS cases

3) To compare these results with the results of the original paper in order to confirm or refute the statements and figures presented in that publication

4) To show any new results which arise from the exact computations.

1 OBLATE SPHEROIDAL WAVE FUNCTIONS

The need to free the derivation of the OS waveguide from the 1P assumption poses some additional complications in the mathematics. Since the wave propagation is not 1P, then one cannot *assume* that the waves will move along the coordinate lines. The boundary condition at the device walls must become an explicit requirement. Rather than belaboring the reader with an in-depth derivation of the OS waveguide equations which contain an explicit angular boundary condition, the author refers the reader to Freehafer [8]. The purpose of this section is to show an updated approach to calculating the OS wave functions, namely numerically, on a computer. In essence these calculations will confirm the work of Freehafer. Later sections will use the results to further the understanding of an OS waveguide by extending the previous works.

1.1 Notation

The literature on OS wave functions is confusing due in no small way to the lack of a consistent notation for the functions. In this paper the notation of Flammer [9] will be used with a few exceptions. Flammer's notation is more widely used than, for instance, Freehafer's, and is generally accepted as the standard. In Flammer's text $i\xi$ is used for the OS functions to indicate the sign difference in the equations which differentiate these functions from the prolate spheroidal functions, for which he uses ξ as the radial parameter. In this paper there is no possibility of confusion between oblate and prolate functions, and so the i is dropped from the ξ specification for convenience. Otherwise the notation here and that in Flammer are identical.

The following are definitions:

ω = angular frequency
$\mathbf{c}$ = wave speed
k = wavenumber, $= \omega/\mathbf{c}$
a = throat radius
θ_0 = angle defining waveguide walls in OS coordinates
$d = \dfrac{2a}{\sin \theta_0}$ = "oblateness" parameter, diameter of the origin (Fig. 1)
c = scaled frequency parameter, $\frac{1}{2}\, kd$
η = OS "angular" variable, $\cos \theta$
ξ OS "radial" variable
g_ξ = scale factor for ξ coordinate [defined in section 2.1]
$S_n(c, \eta)$ = angular wave function of order n (real)
$R_n^{(1)}(c, \xi)$ = radial function of the first kind of order n (real)
$R_n^{(2)}(c, \xi)$ = radial function of the second kind of order n (real)
$R_n^{(3)}(c, \xi)$ = radial function of the third kind of order n (complex, represents outgoing waves), $= R_n^{(1)} + iR_n^{(2)}$.
$W_n(c, \xi)$ = Wronskian [defined in Eq. (3)]
$\Psi(c, \eta, \xi)$ = velocity potential function in OS coordinates
$A_n(c)$ = modal velocity contribution factors
$\Delta_n(c)$ = angular function normalization constant [defined in Eq. (8)]
$v_n(c, \eta, \xi)$ = modal velocity (magnitude in the ξ direction)
$p_n(c, \eta, \xi)$ = modal scalar pressure field
$u_0(\eta)$ = source velocity amplitude
$B_n(c)$ = modal impedance coefficient
$Z_n(c, \eta)$ = modal specific acoustic impedance at point η on source
$z_n(c)$ = complex modal impedance (acoustical)
$Z(c)$ = complex throat impedance function (mechanical)
A = throat area

1.2 Angular Wave Functions

The central problem in the derivation of the OS waveguide is to solve the partial differential equations which describe the wave equation in the OS coordinates. When separated, the equations contain an eigenvalue

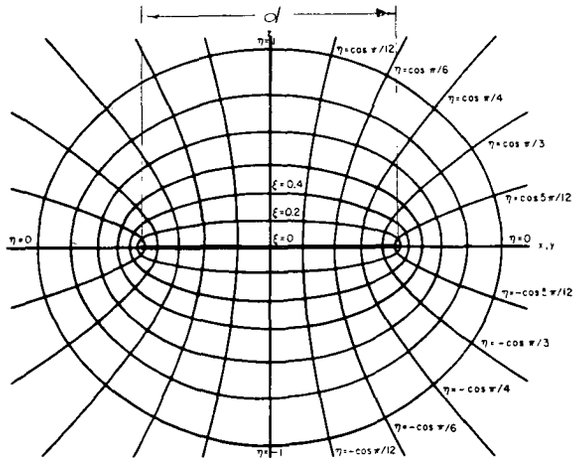

Fig. 1. Oblate spheroidal coordinate system. (From Flammer [8].)

which must be determined. In the case of the OS coordinate system it will be a function of the parameter c. The first step in the solution is to derive the angular wave functions which have zero slope at $\theta = \theta_0$. These calculations will develop the eigenvalues for the particular coverage angle under consideration. The zero slope at $\theta = \theta_0$ means that only even values of n are applicable; odd values of n generate functions having zero value at $\theta = \theta_0$. (The odd set would be useful, for instance, for a pressure release boundary condition.) Freehafer implicitly selects the even set by his choice of boundary condition but defines his angular functions to be of order $n = 0, 1, 2, \ldots$. In this paper the usage of the orders $n = 0, 2, 4, \ldots$ can be seen to be identical. The later usage conforms more closely with the Flammer notation.

The solution of the angular equation can be achieved in a number of ways [10]. The technique which was chosen is a relaxation method. Since the OS equations are identical with the spherical equations for $c = 0$, the solutions are known (Legendre polynomials). Starting with these solutions, the answers for increasing values of c can be built up progressively from zero by using the previous answer as a starting point for the next value of c. In this way very rapid convergence is obtained. An entire set of angular functions can be built up ($n = 0, 2, 4$, $c = 0.0, 12.0$ in 51 steps at 41 angular points) in about 30 s on a 33-MHz 486 PC.

Fig. 2 shows the 30° waveguide angular functions for the extreme values of c calculated, namely, $c = 0.0, 12.0$. This figure is identical to Freehafer's Fig. 3. The angular functions will look nearly identical for any value of θ_0, except that they will change with c at different rates. An examination of Fig. 2 will seem to indicate that these functions *do not* have a slope of zero at $\theta = 0$ ($\eta = \cos\theta = 1.0$) as they must. This is in fact not the case, as Fig. 3 shows. In this figure the angular functions are replotted as a function of θ instead of η. In this paper the θ abscissa will be used.

Fig. 4 shows a plot of the eigenvalues as a function of c^2. These can be compared with Freehafer's eq. (16b) and can be seen to be identical (except that Freehafer uses $-c^2$ for the same reason Flammer uses ic.) The minus sign will be dropped here since it is already included in the differential equation.

1.3 Radial Functions

The next step is to calculate the radial functions. Since the eigenvalues are now known, this becomes a straightforward numerical integration of an ordinary differential equation. From Flammer it can be shown that for the even functions,

$$\frac{d}{d\xi} R_n^{(1)}(c, \xi)\bigg|_{\xi=o} = R_n^{(1)'}(c, 0) = 0 . \qquad (1)$$

Starting with this slope and an assumed value of 1 at $\xi = 0.0$, the function of the first kind can be developed to within a scale factor. This scale factor can then be determined by noting that

$$\lim_{kr\to\infty} R_n^{(1)}(c, \xi), \Rightarrow \lim_{kr\to\infty} j_n(kr)$$

$$= \frac{1}{kr} \cos\left(kr - \frac{n+1}{2}\pi\right) \qquad (2)$$

where $j_n(kr)$ is the spherical Bessel function of order n and r is the radius to the field point. Note that $c\xi$ is analogous to kr and that the two become equivalent at large values.

The scale factor is determined by requiring that the derived functions converge to Eq. (2) for sufficiently large $c\xi$. Figs. 5–7 show the radial functions of the first kind for $n = 0$, 2, and 4, respectively, for several

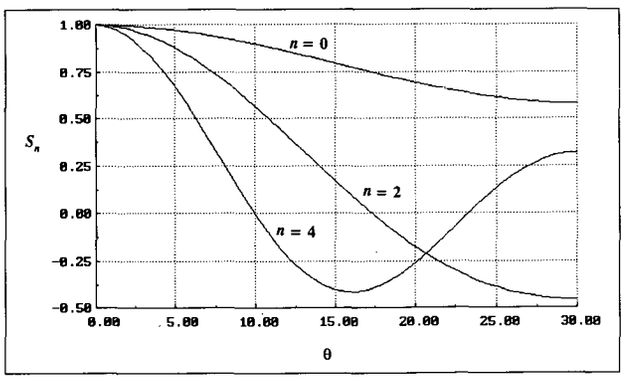

Fig. 3. Angular functions as a function of θ_0. $c = 12.0$.

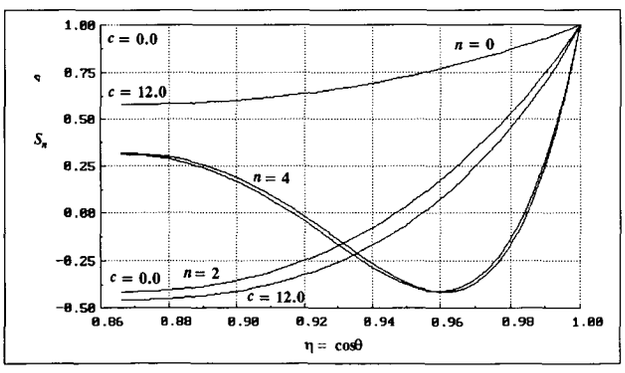

Fig. 2. Oblate spheroidal angular functions for 30° case.

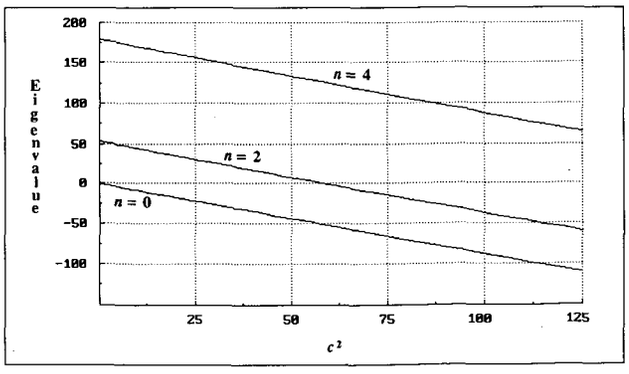

Fig. 4. Eigenvalues for 30° case.

values of c. Calculating a set of these functions (n = 0, 2, 4 at 101 "radial" locations by 51 values of c) takes about 1 min on the PC.

The functions of the second kind are far more complicated to evaluate. The value of the slope at the origin can be determined from Eq. (1) and the value of the Wronskian,

$$W_n(c, \xi) = R_n^{(1)}(c, \xi)\, R_n^{(2)'}(c, \xi) + R_n^{(1)'}(c, \xi)\, R_n^{(2)}(c, \xi) = \frac{1}{c(1 + \xi^2)} \quad (3)$$

at $\xi = 0.0$. This leads to an equation which defines the slope at the origin,

$$R_n^{(2)'}(c, 0) = \frac{1}{cR_n^{(1)}(c, 0)} . \quad (4)$$

Unlike the functions of the first kind, determining the value of $R_n^{(2)}(c, 0)$ is not simply a matter of finding the correct scale factor to ensure an asymptotic form similar to Eq. (2). The boundary conditions of the slope *and* the value of the function must be correct for the integration of the function to converge to the correct asymptotic form. Only one of these conditions is known [Eq. (4)].

A procedure was found which yields the radial function of the second kind of order zero. First a value for $R_n^{(2)}(c, 0)$ is guessed (estimated). Then by comparing the generated function with the asymptotic form for $R_n^{(2)}(c, \xi)$,

$$\lim_{kr\to\infty} R_n^{(2)}(c, \xi) \Rightarrow \lim_{kr\to\infty} n_n(kr) = \frac{1}{kr} \sin\left(kr - \frac{n + 1}{2}\pi\right) \quad (5)$$

where $n_n(kr)$ is the spherical Bessel function of the second kind of order n, a "goodness of fit" parameter can be calculated as the mean squared error between the generated function and the exact function over a range of values of large $c\xi$. Minimizing this error by iterating the value of the function at the origin resulted in convergence of this process to the correct function. Fig. 8 shows this function for several values of c. A single order of these functions (51 values of c and 101 values of $c\xi$, that is, 5151 values of the argument) takes about 2 min on the PC.

The procedure given in the preceding for calculating the radial functions of the second kind was found to be unstable for $n > 0$. The reason for the inability of the method to converge has to do with the extremely large numbers required for the slope and the value of the function at the origin for small values of c. Powers of 10^{12} are typical. The resolution required for convergence turned out to be below the machine's ability to calculate it. Fortunately the functions of the second

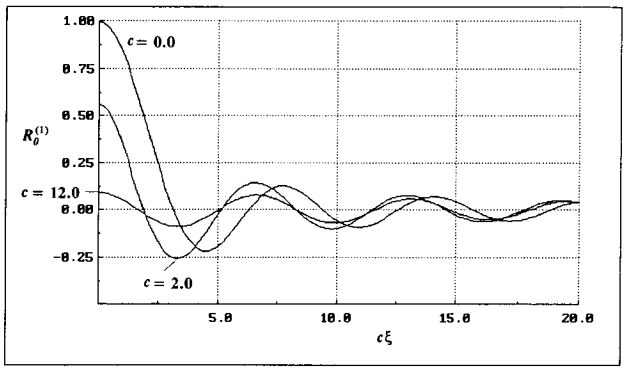

Fig. 5. Radial functions of the first kind of order 0.

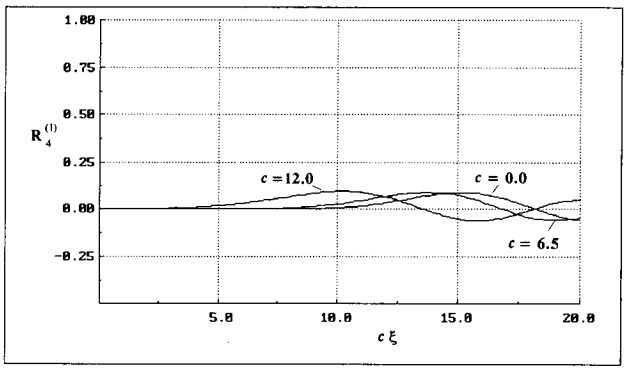

Fig. 7. Radial functions of the first kind of order 4.

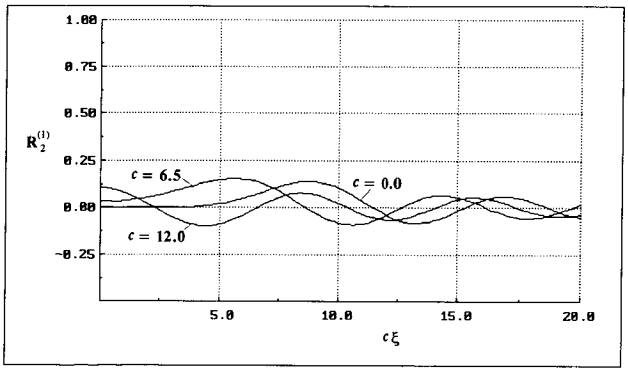

Fig. 6. Radial functions of the first kind of order 2.

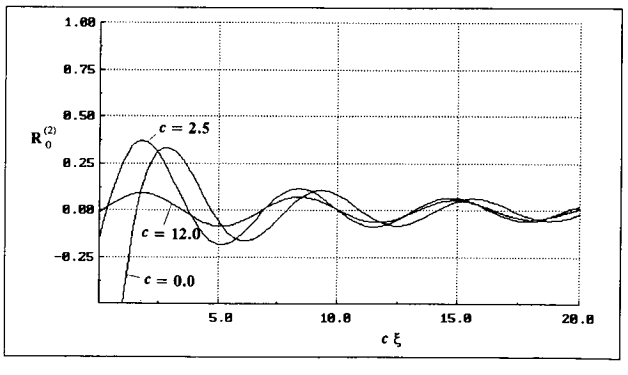

Fig. 8. Radial functions of the second kind of order 0.

kind are not required for the calculations in later sections.

Since the procedures used to derive the set of OS wave functions are all numerical, it is reasonable to estimate their accuracy. The accuracy of the angular functions comes directly from the numerical routines as a convergence parameter. The angular functions are expected to be accurate to about five significant figures. In the case of the radial functions the accuracy was determined in several ways. The first was to continue to reduce the numerical integration tolerance value until no further change in the functions was noted. Further, the value of $c\xi$ necessary for the accuracy of Eqs. (2) and (5) was extended until no change in the frunctions was noted. The final check on the accuracy of the functions (possible only in the $n = 0$ case) was to calculate the Wronskian for the two functions and to compare this function with the exact value. Fig. 9 shows two cases, $c = 0.66$ and $c = 6.6$. From these procedures it is estimated that the radial functions are accurate to about three significant figures.

2 OBLATE SPHEROIDAL WAVEGUIDE EQUATIONS

Once the wave functions in the OS coordinate system (with a boundary condition that the angular velocity at θ_0 is zero) have been calculated, the exact wave motion and impedance characteristics for an arbitrary waveguide can be analyzed. (Only the case of $\theta_0 = 30°$ has been shown, although the software programs have no angular constraint.)

The derivations in this section are very similar to those found in Freehafer. There are some differences, however. The notation difference and the use of exact calculations (Freehafer often uses simplifications) are the most significant, although some new concepts will be introduced. Whenever the details are left out (for brevity), they can be found in Freehafer, considering the differences in notation.

2.1 Velocity Series

The first step in the analysis is to determine the modal contribution coefficients $A_n(c)$ in the equation

$$\psi(c, \eta, \xi) = \frac{d}{2} \sum_{n=o}^{\infty} A_n(c)\, S_n(c, \eta)\, R_n^{(3)}(c, \xi) \ . \qquad (6)$$

Eq. (6) has been defined differently than in Freehafer with the inclusion of the factor $d/2$. This is done for convenience, in order to simplify the A_n. The A_n values can be found from the following equation for the velocity,

$$v_\xi(c, \eta)\Big|_{\xi=0} = \nabla_\xi \psi(c, \eta, \xi)\Big|_{\xi=0}$$

$$= \frac{1}{g_\xi} \frac{d}{d\xi} \psi(c, \eta, \xi)\Big|_{\xi=0} = u_0 f(\eta)$$

where

$$g_\xi = \frac{d}{2} \sqrt{\frac{\xi^2 + \eta^2}{\xi^2 + 1}}$$

which, using Eq. (6), leads to

$$\sum_{n=0}^{\infty} A_n(c)\, S_n(c, \eta)\, R_n^{(3)'}(c, 0) = u_0 \eta\, f(\eta) \ . \qquad (7)$$

The normal velocity of the source is set to the variable $u_0 f(\eta)$ in order to facilitate investigations in later sections. For a rigid piston source, $f(\eta) = 1.0$. From Eq. (7) the A_n are found to be, using the orthogonality of the angular wave functions S_n,

$$A_n(c) = \frac{u_0 \int_{\eta_0}^{1} S_n(c, \eta)\, \eta f(\eta)\, d\eta}{\Delta_n(c)\, R_n^{(3)'}(c, 0)} \ .$$

Using Eq. (4) and the definition of $R_n^{(3)}$ leads to

$$A_n(c) = -\frac{iu_0\, c\, R_n^{(1)}(c, 0) \int_{\eta_0}^{1} S_n(c, \eta)\, \eta f(\eta)\, d\eta}{\Delta_n(c)} \ . \qquad (8)$$

In these equations,

$$\Delta_n(c) = \int_{\eta_0}^{1} S_n^2(c, \eta)\, d\eta$$

is the normalization constant for the angular functions. Note in Eq. (8) that the A_n depend only on the radial functions of the first kind.

The values of $A_n(c)$ can be used to find the wave propagation at any point in the waveguide as long as the radial functions of the second kind are known or assumed to be insignificant. Of most interest is the waveshape at the mouth, since this shape will determine the directivity of the device. By considering the radial

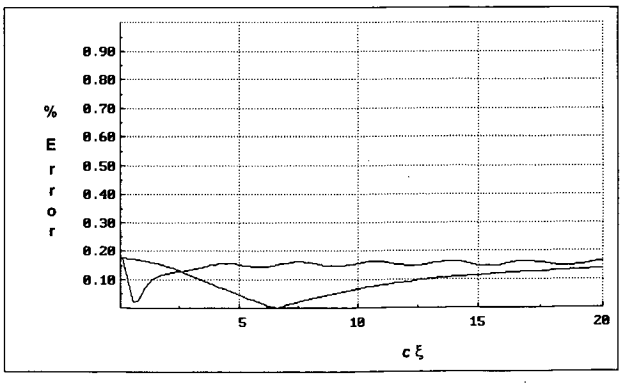

Fig. 9. Wronskian error for $n = 0$.

functions for large values of $c\xi$ we can determine a simple form for the series of wave functions at the mouth which does not require the functions of the second kind. The following asymptotic approximations will be used,

$$\lim_{c\xi\to\infty} R_n^{(3)}(c, \xi) \Rightarrow \frac{i^{-n-1}}{c\xi} e^{ic\xi} . \quad (9)$$

Using these forms in the equation for the velocity,

$$v_\xi(c, \eta, \xi) = \sum_{n=0}^{\infty} A_n(c)\, S_n(c, \eta)\, R_n^{(3)'}(c, \xi) \quad (10)$$

will yield the velocity at the mouth, assuming a sufficiently long waveguide,

$$v_\xi(c, \eta, \xi)\Big|_{\text{mouth}} = \frac{e^{ic\xi}}{\xi} \sum_{n=0}^{\infty} i^{-n} A_n(c)\, S_n(c, \eta) . \quad (11)$$

Eq. (11) says in essence that the same makeup of the velocity modal contributions that exists at the throat will exist at the mouth, except that the sign of every other mode will be changed. Specifically, the $n = 0$ mode will appear at the mouth with an amplitude which is simply diminished by the distance traveled (essentially the free-space Green's function) but will otherwise remain unaffected. The $n = 2$ mode will travel with the same amplitude reduction, but will add to the $n = 0$ mode with a reversed sign. The $n = 4$ mode (if it is significant) will add with sign unchanged. These results will be used later when the wave propagation for various waveguide configurations is studied.

2.2 Impedance Functions

A useful function is the radiation impedance seen by the source (throat impedance). The real part of this impedance is equal to the power radiated by the source for a unit velocity source. The radiation impedance can be determined directly from the wave functions.

It will be instructive to derive a somewhat different form of the impedance function called the modal impedance $Z_n(c)$. This is done by considering the impedance of a particular mode n at a point on the source,

$$Z_n(c, \eta, \xi)\Big|_{\xi=0} = \frac{p_n(c, \eta, \xi)}{v_n(c, \eta, \xi)}\Big|_{\xi=0}$$

$$= i\rho c \frac{kd}{2} \eta \frac{A_n(c)\, S(c, \eta)\, R_n^{(3)}(c, 0)}{A_n(c)\, S(c, \eta)\, R_n^{(3)'}(c, 0)}$$

$$= i\rho c \frac{kd}{2} \eta \frac{R_n^{(3)}(c, 0)}{R_n^{(3)'}(c, 0)}$$

which, after using Eq. (4), leads to

$$Z_n(c, \eta) = \rho c \eta c^2 R_n^{(1)}(c, 0)\, [R_n^{(1)}(c, 0) + iR_n^{(2)}(c, 0)] . \quad (12)$$

To obtain the average impedance in the plane of the source, the preceding result must be integrated over the surface of the source and divided by the total area. (Freehafer shows how this can be done.) Dividing this average impedance by ρc yields the dimensionless quantity $z_n(c)$, which will be called the normalized modal impedance at the throat. These calculations yield

$$z_n(c) = \frac{2(1 - \cos^3 \theta_0)}{3 \sin^2 \theta_0} c^2 R_n^{(1)}(c, 0) \times [R_n^{(1)}(c, 0) + iR_n^{(2)}(c, 0)] . \quad (13)$$

This last form will be particularly insightful in future discussions.

With regard to the modal impedance, it will be useful to define a set of modal weights $B_n(c)$ in such a way that

$$\sum_n B_n(c)\, z_n(c) = \frac{Z(c)}{A\rho c} \quad (14)$$

where $Z(c)$ is the mechanical radiation impedance defined in Freehafer. A comparison of Eqs. (13) and (14) with Freehafer's Eq. (6) means that

$$B_n(c) = \frac{3}{(1 - \cos^3 \theta_0)\Delta_n(c)} \left[\int_{z_0}^{1} S_n(c, \eta)\, \eta f(\eta)\, d\eta\right]^2 . \quad (15)$$

The $B_n(c)$ are dimensionless. Since the impedance is proportional to the power transfer of the waveguide, the $B_n(c)$ will represent the acoustic power contained in each mode.

Note in Eq. (13) that the real part of the impedance function depends only on the radial function of the first kind. The imaginary part of z_n (the mass reactance) can be calculated only for the $n = 0$ case. If the imaginary part for the higher-order modes $n > 0$ is desired, it can be determined by the Kramers–Kronig relationship [11]. Incidentally, the value of the radial function of the second kind at the origin could be determined from the value of the imaginary part of the radiation resistance as determined from the Kramers–Kronig relationship. In this way a possible method for the calculation of the radial functions of the second kind is revealed. This will not be done in this paper. As we shall see, as far as the impedance is concerned, it is usually sufficient to exclude all but the zeroth-order mode.

Now that the necessary equations have been developed, several particular devices can be investigated in detail.

3 OBLATE SPHEROIDAL WAVEGUIDE EXAMPLES

3.1 15° Oblate Spheroidal Waveguide

While not particularly useful due to its narrow coverage (30° total angle), the 15° waveguide will offer some insights into the general characteristics of OS waveguides. It will also be used to present the data format for the next set of examples. The data in the case of the 15° device have been included for completeness and for comparison with the other devices studied.

In the 15° waveguide virtually the only mode excited is $n = 0$. For this device the highest practical value of c that needs to be considered is $c = ka/\sin\theta_0 \cong 11.0$ for a 1-in (25.4-mm) diameter throat at 12 kHz (hence the choice of range for the analysis). These values of c will correspond to even higher frequencies for wider pattern waveguides. The acoustic modal impedance functions are shown in Fig. 10. The only impedance of significance is the $n = 0$ mode, the other modes having negligible values in the range of c shown. For this waveguide the modal impedance [Eq. (13)] and the total impedance (from Freehafer's fig. 6), are nearly identical. The difference is due to Freehafer's approximations for the larger values of c.

The modal velocity contribution factors $A_n(c)$ are shown in Fig. 11. This figure assumes an axially vibrating source. The modal velocity contribution factor, in light of Eq. (11), can be thought of as a velocity transfer function from the throat to the mouth (except for the sign of the terms).

Fig. 12 gives the modal impedance coefficients $B_n(c)$, verifying the statement that only the $n = 0$ case is relevant. Fig. 13 shows the mouth velocity as a function of θ. In these figures it can be seen that only a minimum of "non-1P" behavior is evident. For a 15° waveguide the assumption of 1P behavior is very accurate for any useful frequency range.

3.2 30° Oblate Spheroidal Waveguide

Performing the same calculations as in Section 3.1 for a 30° waveguide yields Figs. 14–17 for the modal impedance, the modal velocity coefficients, the modal impedance coefficients, and the mouth velocity, respectively. Here we begin to see the appearance of a new phenomenon. The second mode, $n = 2$, has a cutoff frequency at about $c = 7.5$. The appearance of higher order modes which have individual cutoff frequencies is a significant result not previously recognized.

The 30° waveguide is not a 1P device at the extreme high-frequency end of the range shown [about 23 kHz for a 1-in (25.4-mm) throat]. It is very nearly a 1P device below the second-mode cutoff frequency [about 16 kHz for a 1-in (25.4-mm) throat]. This waveguide points out a very interesting result of the presence of the higher order modes. Waves corresponding to these modes do not propagaete below their individual cutoff frequencies. The waves for these nonpropagating modes

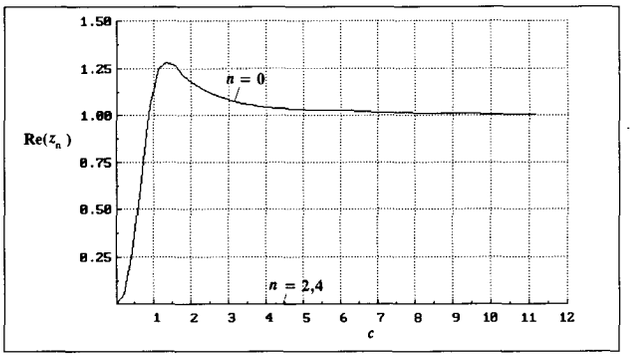

Fig. 10. Modal impedances for 15° waveguide.

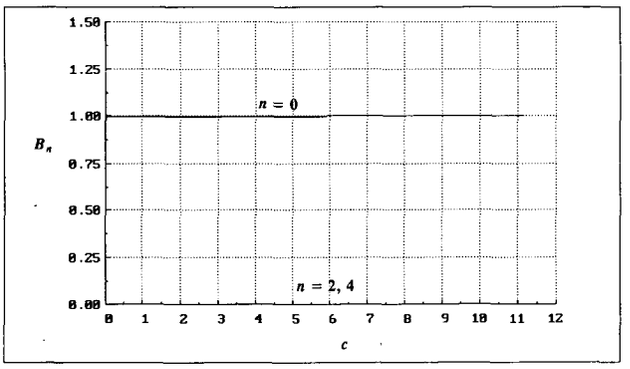

Fig. 12. Modal impedance coefficients for 15° waveguide.

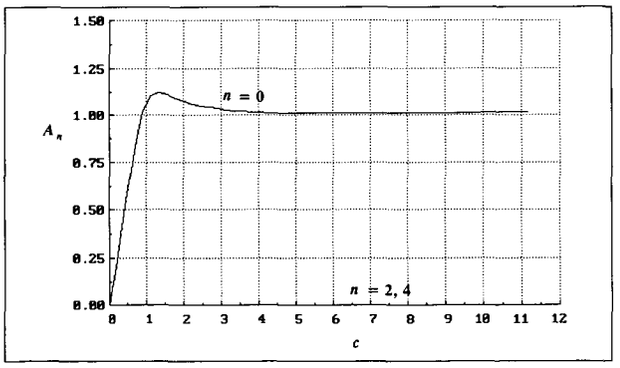

Fig. 11. Modal velocity coefficients for 15° waveguide.

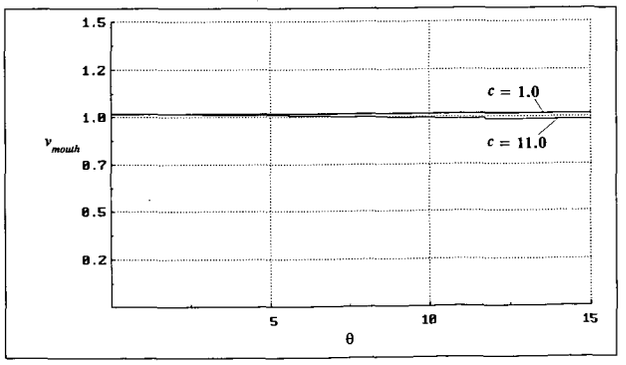

Fig. 13. Mouth velocity for 15° waveguide.

are known as evanescent waves. They decay exponentially away from the throat, becoming negligibly small at the mouth.

A positive result of the modal cutoff is that, unlike the author's previous belief, the mouth need not be fed with an exact plane wave for good results. The mode cutoff phenomenon has the effect that up to the second-mode cutoff frequency the waveguide will filter out all of the higher order modes, passing only the $n = 0$ mode. This effect will likewise occur for each successive mode; the waveguide will filter out all higher order modes until their individual cutoff frequencies have been passed. In essence, since the cutoff frequency for the $n = 4$ case is so high, only those throat velocity components which influence the $n = 0, 2$ waves will ever be of any significance at the mouth. This is an interesting and significant result. These observations should not be surprising since an exactly analogous effect is found for wave propagation in ducts [12].

3.3 45° Oblate Spheroidal Waveguide

The characteristics for a 45° waveguide are shown in Figs. 18–21. It is interesting to note that the second-mode cutoff is at nearly the same frequency as in the 30° waveguide (although at a different c value). The third mode is beginning to appear at the upper frequencies. Again it can be seen that no major effect of the higher order modes is seen at frequencies below that mode's cutoff. The 1P assumption is a good approximation for a 45° waveguide to about 12 kHz for a 1-in (25.4-mm) throat. Above this frequency, however, major deviations from the 1P assumption occur.

3.4 Source Velocity Modifications

After considering the general characteristics for three waveguides which have been driven at the throat by a uniform velocity source, that is, $f(\eta) = 1.0$, a good question would be; Is there a way to further suppress the higher order modes with a proper choice of source velocity? It turns out that this is in fact a very viable option. Fig. 22 shows the throat velocity such that

$$v_\xi(c, \eta, 0) = f(\eta) = \frac{S_0(c = 7.0, \eta)}{\eta} . \qquad (16)$$

Note in Fig. 23 how this choice of source velocity distribution has caused the second-mode velocity contribution to be zero at $c = 7.0$ and that is possesses opposite signs above and below this point. The significance of this result can be seen in Fig. 24. When compared with Fig. 21, a 45° waveguide with uniform throat velocity, it can be seen that a significant reduction in the beaming (or non-1P performance) has occurred. The scales of Figs. 21 and 24 have been kept the same for ease of comparison. The lower average velocity at the mouth is a result of the lower average velocity of the source (from Fig. 22). It can be seen that a careful design of the phasing plug could be used to extend the range over which an OS waveguide is effectively a 1P device.

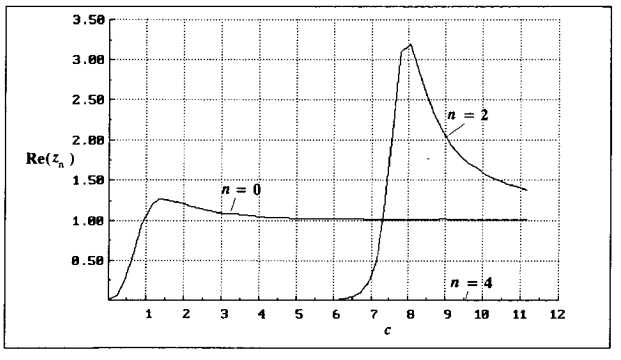

Fig. 14. Modal impedances for 30° waveguide.

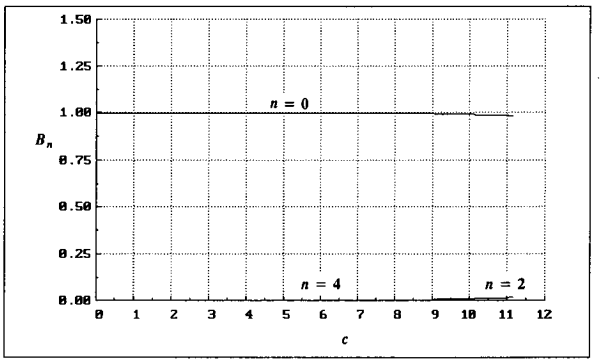

Fig. 16. Modal impedance coefficients for 30° waveguide.

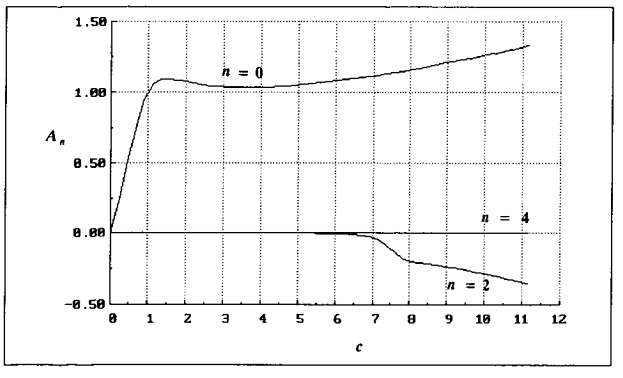

Fig. 15. Modal velocity coefficients for 30° waveguide.

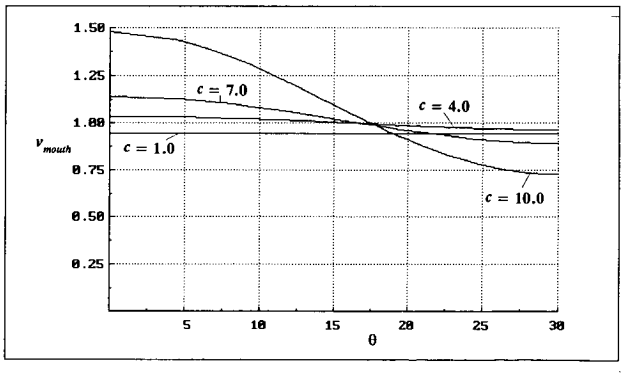

Fig. 17. Mouth velocity for 30° waveguide.

3.5 A Note on Directivity

The principal purpose of this paper has been to develop a solution of the wave equation *in* a waveguide. The motivation for this solution is to determine the velocity distribution at the mouth of the device. Once this velocity distribution is known, the directivity can be determined. The actual far-field directivity for the examples shown has not been calculated.

The calculation of the directivity (far-field response) of an acoustic aperture has been discussed at length in other papers [11], [13], [14]. Of particular importance here is whether or not the waveguide is aperture diffraction limited or limited by the "beaming" of the sound field so that significant aperture diffraction will not exist. In [13] it was shown that the directivity is strongly influenced by the aperture diffraction when

$$kR > \frac{15.0}{\sin^2 \theta_0}$$

where R is the length of the device.

Above this frequency, which was called the aperture diffraction limit, the mouth velocity profile will still be an indicator of the directivity, but the response will suffer various aperture diffraction effects which depend more on the details of the aperture than on the velocity profile at the mouth. An example of these effects is the appearance of a "hole" in the axial response which does not exist in the mouth velocity response of a circular waveguide. The off-axis response of a waveguide will basically be that of the mouth velocity profile, although diffraction effects will modify it. This effect is well documented experimentally in [2] and analytically in [13].

4 CONCLUSIONS

This paper has developed several key points. It has been shown:

1) That an exact calculation of the wave propagation in a horn is possible if one resorts to the use of the wave equation instead of Webster's equation. Only a few coordinate geometries and hence waveguide types allow this solution approach. The well-known exponential is not one of them.

2) That in spite of errors which were made in the original waveguide paper the conclusions of that work have been verified to be correct in all but the most extreme cases. The 1P assumption is accurate for all waveguides at lower frequencies and for narrow waveguides at any audio frequency. The limiting frequency for 1P propagation becomes lower for wider directivity waveguides.

3) That departure from 1P behavior is mostly due to the presence of higher order modes. The presence of these higher order modes is a new discovery, and they have significant implications:

- They have cutoff frequencies below which they will not propagate; thus the waveguide acts as a filter of non-1P behavior.
- They occur at a relatively constant frequency for all

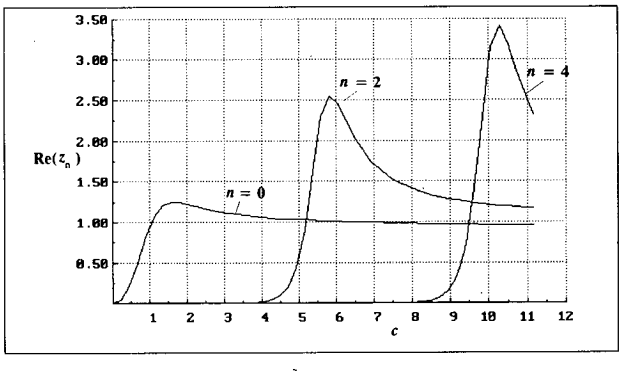

Fig. 18. Modal impedances for 45° waveguide.

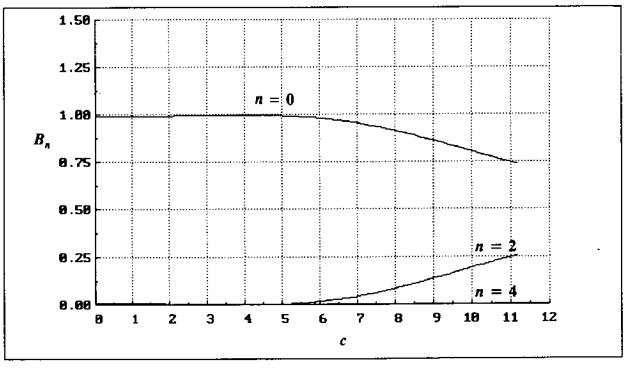

Fig. 20. Modal impedance coefficients for 45° waveguide.

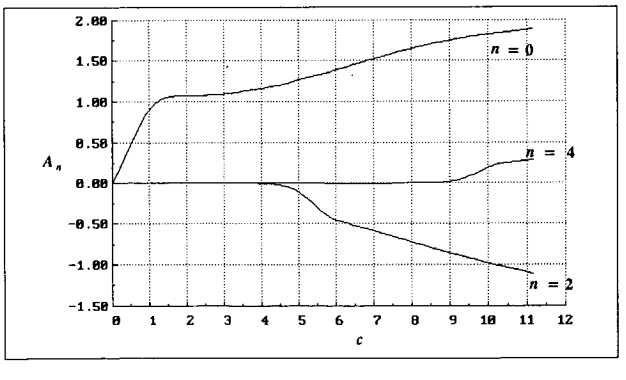

Fig. 19. Modal velocity coefficients for 45° waveguide.

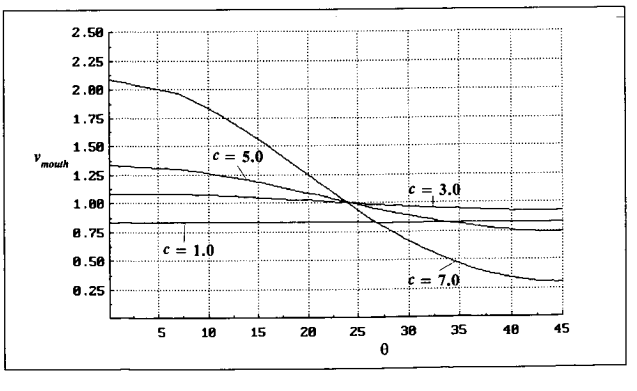

Fig. 21. Mouth velocity for 45° waveguide.

device angles, basically when the wavelength of sound fits across the throat.

- They are not predicted by Webster's equation, although any waveguide whose boundary is an equicoordinate surface in a separable coordinate system must have higher order modes. In nonseparable coordinate systems the usual meaning of higher order modes is lost, although it seems likely that an analog of such modes must exist in any device. The inability of Webster's equation to predict higher order modes means that they cannot be evaluated and hence controlled, a significant shortcoming of the Webster approach.

The waveguide theory, and in particular the OS waveguide, remains a very effective approach to the design of a constant-directivity controlling device.

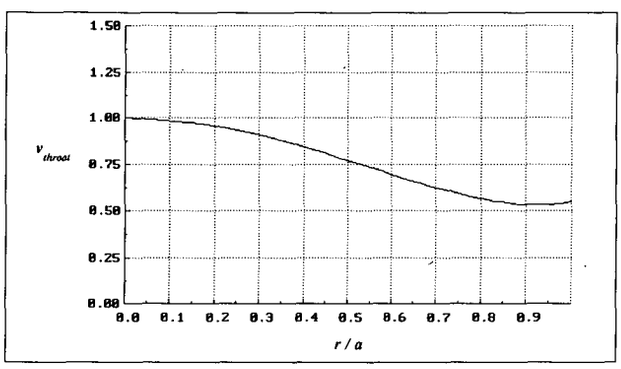

Fig. 22. Throat velocity for optimized 45° waveguide.

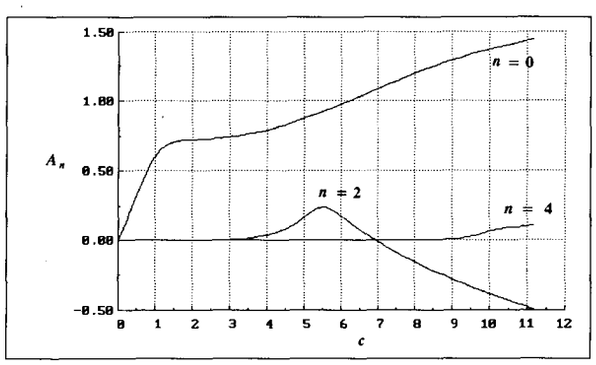

Fig. 23. Modal velocity coefficients for optimized 45° waveguide.

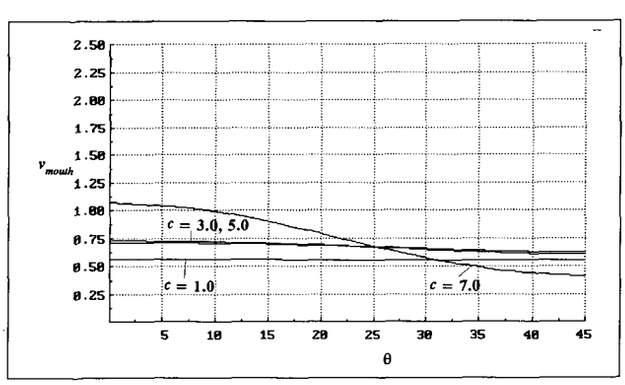

Fig. 24. Mouth velocity for optimized 45° waveguide.

5 ACKNOWLEDGMENT

The author is indebted to all the readers who took the time to comment on his original paper, but a particular debt is owed to Mr. Gavin Putland. His thorough reading of the text and his patient discussions, both public and private, were a continual source of insight and inspiration. The current paper would probably never have been produced if it had not been for Mr. Putland's comments, for without accepting his critique as correct, there would have been no need for this follow-up.

6 REFERENCES

[1] E. R. Geddes, "Acoustic Waveguide Theory," *J. Audio Eng. Soc.*, vol. 37, pp. 554–569 (1989 July/Aug.).

[2] P. D. Bauman, A. B. Adamson, and E. R. Geddes, "Acoustic Waveguides—In Practice," *J. Audio Eng. Soc.*, vol. 41 (this issue).

[3] G. R. Putland, and E. R. Geddes, "Comments on 'Acoustic Waveguide Theory'," *J. Audio Eng. Soc. (Letters to the Editor)*, vol. 39, pp. 469–472 (1991 June) and personal communications.

[4] D. J. Henwood, "Further Comments on 'Acoustic Waveguide Theory'," private communication (1992 May).

[5] G. R. Putland, "Every One-Parameter Acoustic Field Obeys Webster's Horn Equation," *J. Audio Eng. Soc.*, vol. 41 (this issue).

[6] P. M. Morse, *Vibration and Sound* (American Institute of Physics, New York).

[7] E. Geddes and D. Clark, "Computer Simulation of Horn-Loaded Compression Drivers," *J. Audio Eng. Soc. (Engineering Reports)*, vol. 35, pp. 556–566 (1987 July/Aug.).

[8] J. E. Freehafer, "The Acoustical Impedance of an Infinite Hyperbolic Horn," *J. Acoust. Soc. Am.*, vol. 11 (1940 Apr.).

[9] C. Flammer, *Spheroidal Wave Functions* (Stanford University Press, Stanford, CA, 1957).

[10] W. H. Press et al. *Numerical Recipes* (Cambridge University Press, London, 1986).

[11] E. R. Geddes, "Source Radiation Characteristics," *J. Audio Eng. Soc. (Engineering Reports)*, vol. 34, pp. 464–478 (1986 June).

[12] A. D. Pierce, *Acoustics* (McGraw-Hill, New York, 1981).

[13] E. R. Geddes, "Sound Radiation from Acoustic Apertures," *J. Audio Eng. Soc.*, vol. 41, pp. 214–230 (1993 Apr.).

[14] E. R. Geddes, "On the Use of the Hankel Transform for Sound Radiation," presented at the 93rd Convention of the Audio Engineering Society, *J. Audio Eng. Soc. (Abstracts)*, vol. 40, p. 1054 (1992 Dec.), preprint 3428.

The biography for Earl R. Geddes was published in the April issue.